mathematics

MDPI

Article

Conjugate Natural Convection of a Hybrid Nanofluid in a Cavity Filled with Porous and Non-Newtonian Layers: The Impact of the Power Law Index

Mohamed Omri [1], Muhammad Jamal [2], Shafqat Hussain [3,4], Lioua Kolsi [5,*] and Chemseddine Maatki [6]

1 Deanship of Scientific Research, King Abdulaziz University, Jedda 21589, Saudi Arabia; omrimoha2002@yahoo.fr
2 Department of Mathematics & Statistics, PMAS-Arid Agriculture University, Rawalpindi 46300, Pakistan; jamal@uaar.edu.pk
3 Department of Mathematics, Capital University of Science and Technology, Islamabad 44000, Pakistan; shafqat.hussain@cust.edu.pk
4 Institut für Angewandte Mathematik (LS III), Technische Universität, 44227 Dortmund, Germany
5 Department of Mechanical Engineering, College of Engineering, Ha'il University, Ha'il 81451, Saudi Arabia
6 Mechanical Engineering Department, College of Engineering, Al Imam Mohammad Ibn Saud Islamic University, Riyadh 11432, Saudi Arabia; casmaatki@imamu.edu.sa
* Correspondence: lioua_enim@yahoo.fr

Abstract: This study deals with the effect of the power law index on the convective heat transfer of hybrid nanofluids in a square cavity divided into three layers. The effect of a solid fluid layer is also given attention. A two-dimensional system of partial differential equations is discretized by using the generalized finite element method (FEM). A FEM having cubic polynomials (P3) is employed to approximate the temperature and velocity components, whereas the pressure is approached using quadratic finite element functions. The discretized set of equations have been solved using Newton's method. The numerical code which is used in this study has been validated by comparing with experimental findings. Mathematical simulations are performed for different sets of parameters, including the Rayleigh number (between 10^3 and 10^6), the power law index (between 0.6 to 1.8), Darcy number (between 10^{-6} to 10^{-2}), undulation (between 1 and 5) and the thermal conductivity ratio (between 0.1 and 10). The results infer that a remarkable penetration of streamlines is figured out towards the porous hybrid layer as the power law index is increased. The average Nu increases with increasing Ra, and the maximum value is noted at $Ra = 10^6$. There is no much alteration observed for isotherms at the solid layer by increasing Da. The average Nu decreases by increasing the undulations. The rate of heat transfer is enhanced at the heated boundary and solid fluid interface of the cavity by raising the ratio of thermal conductivity.

Keywords: natural convection; hybrid nanofluids; power law; porous medium; layers; Galerkin FEM

MSC: 35Q30

check for updates

Citation: Omri, M.; Jamal, M.; Hussain, S.; Kolsi, L.; Maatki, C. Conjugate Natural Convection of a Hybrid Nanofluid in a Cavity Filled with Porous and Non-Newtonian Layers: The Impact of the Power Law Index. *Mathematics* **2022**, *10*, 2044. https://doi.org/10.3390/math10122044

Academic Editors: Emma Previato and Xiangmin Jiao

Received: 17 April 2022
Accepted: 7 June 2022
Published: 13 June 2022

1. Introduction

Nanofluids are considered to be an innovative key factor allowing the enhancement of heat transfer in many industrial thermal systems. The most commonly used nanoparticles are TiO_2, $MWCNTs$, Al_2O_3, SiO_2 CuO, MgO and Ag. Nanoparticles are used for the synthesis of nanofluids. Some related works are available in the literature [1–9]. The mixture of more than on type of nanoparticle within a base fluid is called a hybrid nanofluid. Porous layers are used to control the heat transfer due to the important heat transfer surface between the fluid and the matrix and convective heat transfer inside pores [10]. Therefore, the analysis of heat transfer in complex domains including Newtonian and non-Newtonian layers and porous layers is very important and useful for the optimization of various engineering applications [11]. In addition, wavy walls lead to higher heat transfer rates compared to flat walls by increasing the exchange surface within the same thermal system.

Esfe et al. [12] used hybrid nanofluids (Ag–MgO/water), with the volume concentration of nanoparticle samples reaching up to 2%. The proportions of Ag and MgO nanoparticles were 50% each. The sizes of the silver and magnesium oxide nanoparticles were 25 nm and 40 nm, respectively. In this study, the dynamic viscosity and thermal conductivity of the hybrid nanofluid were measured for different volume fractions of nanoparticles. Similar studies have been done by Esfe et al. [13] for CNT–Al_2O_3/water hybrid nanofluids and ref. [14] for DWCNT–ZnO/water hybrid nanofluids.

The study of conjugate heat transfer plays an essential role in engineering, including regarding heat transfer between a solid container and a liquid, heat transfer between a heat sink and its nearby fluid, and heat transfer between the thick solid walls of a tube that is filled with liquid. The unsteady natural convection of nanofluids in a porous cavity is studied by Sher. et al. [15]. Sher. and Pop [16] investigated the conjugate heat transfer of non-uniformly distributed nanofluids in a porous medium. Conjugate natural convection in a cavity was examined by Sher. et al. [17]. Due to the worthwhile manufacturing applications of conjugate heat transfer, its characteristics have already been studied in past years [18–23].

Alsabery et al. [24] considered a trapezoidal-shaped cavity including two layers: a porous layer and a non-Newtonian layer. The results confirmed that the flow rose considerably using silver nanofluid, and the effectiveness in heat transfer was also enhanced by varying the angle of inclination. Rashid and Ali. [25] reported on the impact of Pr on the natural convection in a cavity containing non-Newtonian and nanofluid porous medium separated by a sinusoidal interface. It has been figured out that the average Nu rises by enhancing the Darcy and Pr and reduces by enriching n.

Power law fluids have been the focus of researchers and scientists due to their importance in engineering, such as in polymer engineering, as heat exchangers, as chemical catalytic reactors and in geothermal systems [26]. More details can be found in [27–35].

Alsabery et al. [36] numerically investigated the effects of fluid layers and inclination angle on natural convection. The results show that convection is notable with lower values of n, and it drops when n increases. The impact of a wavy interface on natural convection in a non-Darcy porous cavity has been studied by Nguyen et al. [37] using the ISPH method. The results indicated that the average Nu declines by increasing the amplitude and undulation number of the interface which is located among the layers.

The impact of heated walls with porous layers on natural convection has been investigated by Al-Srayyih et al. [38] by employing GFEM. It has been observed that heat transfer increases at low values of thermal conductivity. Additionally, a higher rate of heat transfer has been found using hybrid nanofluids. Jabber et al. [39] investigated the impact of a wavy wall in a square enclosure with a non-Newtonian nanofluid and porous medium. The findings reveal that the average Nu decreases when n increases. Furthermore, the thicknesses of layers have an important effect on the heat transfer rate, while the impact of the number of undulations is negligible.

Natural convection in a 2D cavity having a wavy wall and filled with a power law fluid was studied by Chen et al. [40]. The authors mentioned that the rate of heat transfer of a pseudo-plastic fluid is more intense than that of a Newtonian fluid. Kefayati et al. [41] applied LBM to figure out the behaviour of non-Newtonian fluid during natural convection under the effect of an external uniform magnetic field. The results indicated that when n and Ha rise, the heat transfer is reduced considerably, while it is significantly enhanced for high buoyancy ratio values.

Saleh et al. [42] discussed the natural convection in polygon-shaped cavities including a rotating obstacle by using COMSOL. It has been found that the heat transfer rate remains steady at $L/D > 0.77$ and no considerable change is encountered in the variations of Nu. Turan et al. [43] considered the natural convection of non-Newtonian fluids in a 2D cavity having two active vertical walls. The authors proposed some new correlations relating Pr

and *Ra* numbers, allowing the direct evaluation of the heat transfer rates for the Newtonian and non-Newtonian fluids.

Barnoon et al. [44] analysed the combined effects of radiation and convection on the flow in an enclosure based on the two phases model. The results revealed that the cavity inclination has an important effect on the flow structure and the heat transfer rate.

Based on the above-described literature review, it is clear that no studies have been done on the effect of wavy interfaces in a square cavity filled with a hybrid nanofluid and including three layers (solid, porous and non-Newtonian). The current study represents an effort to report the above combination in a comprehensive way. The applications of this study are in engineering and industry where the layers are involved. The study focuses on the effect of increasing the layers and the other controlling parameters, such as the Rayleigh number, power law index, Darcy number, undulations and ratio of thermal conductivity on the flow structure, temperature field and heat transfer.

2. Mathematical Model

2.1. Geometry of the Considered Problem

The configuration considered in the present study is shown in Figure 1. It consists of a 2D differentially heated squared cavity filled with a hybrid nanofluid and composed of three layers.

- L and H are the length and height, respectively;
- T_h and T_c are the temperatures on the left and right walls, respectively. The remaining walls are considered to be adiabatic;
- $H1$ is the width of the conjugate layer, and $H2 - H1$ is the width of the porous hybrid layer;
- The solid wavy interface is derived from the following equation: $x = H1 + A\,sin(2N\pi y)$, where $H1 = 0.1$;
- The porous wavy interface is derived from the following equation: $x = H2 + A\,sin(2N\pi y)$, where $H2 = 0.2$;
- Three layers are considered in this study;
- The flow is considered steady, laminar, and incompressible;
- The thermophysical properties of Ag/MgO-water are given in Table 1.

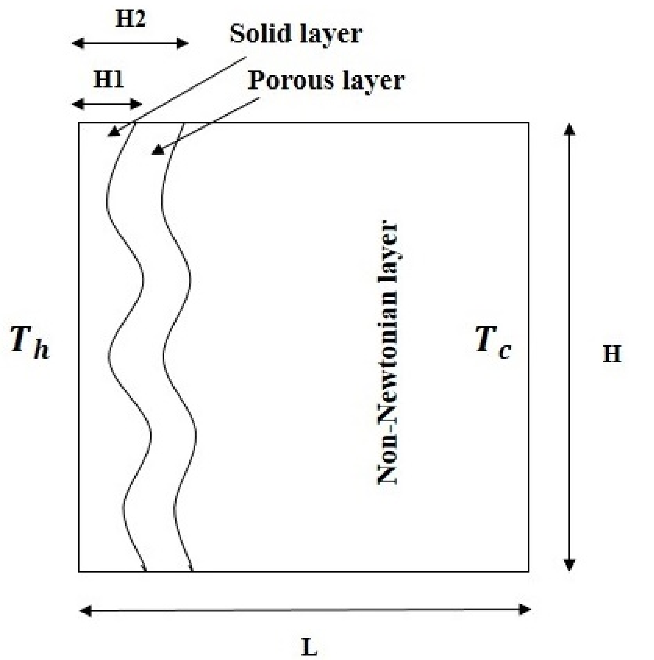

Figure 1. Computational sketch of the present problem.

Table 1. Thermophysical properties of alumina and copper [45,46].

Properties	Ag	MgO	Water
ρ (kg/m^3)	10,500	3580	997.1
C_p (J/kgK)	235	879	4179
k (W/mK)	429	30	0.613
β (1/K)	5.4×10^{-5}	33.6×10^{-6}	21×10^{-5}
μ (kg/ms)	—	—	8.9×10^{-4}
α (m^2/s)	174×10^{-3}	95.3×10^{-7}	1.47×10^{-7}

2.2. Formation of Equations

Based on the above mentioned assumptions, the dimensional governing equations are written as [46–48]:

For the non-Newtonian nanofluid layer:

$$\frac{\partial u}{\partial x} + \frac{\partial v}{\partial y} = 0 \text{ (continuity equation)}, \tag{1}$$

$$\rho_{hnf}\left(u\frac{\partial u}{\partial x} + v\frac{\partial u}{\partial y}\right) = -\frac{\partial p}{\partial x} + \mu_{hnf}\left(\frac{\partial \tau_{xx}}{\partial x} + \frac{\partial \tau_{xy}}{\partial y}\right) \text{ (u-momentum equation)}, \tag{2}$$

$$\rho_{hnf}\left(u\frac{\partial v}{\partial x} + v\frac{\partial v}{\partial y}\right) = -\frac{\partial p}{\partial y} + \mu_{hnf}\left(\frac{\partial \tau_{xy}}{\partial x} + \frac{\partial \tau_{yy}}{\partial y}\right) + (\rho\beta)_{hnf} g(T - T_c) \text{ (v-momentum equation)}, \tag{3}$$

$$u\frac{\partial T}{\partial x} + v\frac{\partial T}{\partial y} = \alpha_{hnf}\left(\frac{\partial^2 T}{\partial x^2} + \frac{\partial^2 T}{\partial y^2}\right) \text{ (energy equation)}. \tag{4}$$

For Cartesian 2D coordinates, the shear stress tensor (based on the power law model) has been known by the relation given below [47]:

$$\tau_{ij} = 2\bar{\mu}_\alpha D_{ij} = \bar{\mu}_\alpha\left(\frac{\partial u_i}{\partial x_j} + \frac{\partial u_j}{\partial x_i}\right), \tag{5}$$

where D_{ij} is the strain rate and $\bar{\mu}_\alpha$ symbolizes the apparent viscosity, written as follows:

$$\bar{\mu}_\alpha = m\left[2\left\{\left(\frac{\partial u}{\partial x}\right)^2 + \left(\frac{\partial v}{\partial y}\right)^2\right\} + \left(\frac{\partial v}{\partial x} + \frac{\partial u}{\partial y}\right)^2\right]^{\frac{n-1}{2}}. \tag{6}$$

For the Newtonian nanofluid porous layer:

$$\frac{\partial u}{\partial x} + \frac{\partial v}{\partial y} = 0, \tag{7}$$

$$\frac{\rho_{hnf}}{\epsilon^2}\left(u\frac{\partial u}{\partial x} + v\frac{\partial u}{\partial y}\right) = -\frac{\partial p}{\partial x} + \frac{\mu_{hnf}}{\epsilon}\left(\frac{\partial^2 u}{\partial x^2} + \frac{\partial^2 u}{\partial y^2}\right) - A_x, \tag{8}$$

$$\frac{\rho_{hnf}}{\epsilon^2}\left(u\frac{\partial v}{\partial x} + v\frac{\partial v}{\partial y}\right) = -\frac{\partial p}{\partial y} + \frac{\mu_{hnf}}{\epsilon}\left(\frac{\partial^2 v}{\partial x^2} + \frac{\partial^2 v}{\partial y^2}\right) + (\rho\beta)_{hnf} g(T - T_c) - A_y, \tag{9}$$

$$u\frac{\partial T}{\partial x} + v\frac{\partial T}{\partial y} = \alpha_{hnf}\left(\frac{\partial^2 T}{\partial x^2} + \frac{\partial^2 T}{\partial y^2}\right), \tag{10}$$

$A = (A_x, A_y)$ is known the force term due to the Darcy–Forchheimer porous medium; it is assumed by the equation below [48]:

$$(A_x, A_y) = \left(\frac{\mu_{hnf}}{K} + \frac{\rho_{hnf} F_c}{\sqrt{K}}\left(\sqrt{u^2 + v^2}\right)\right)(u, v), \tag{11}$$

where

$$K = \frac{\epsilon^3 d^2}{150(1-\epsilon)^2},$$

$$F_c = \frac{1.75}{\sqrt{150\epsilon^2}}.$$

For the solid layer:

$$k_s\left(\frac{\partial^2 T_s}{\partial x^2} + \frac{\partial^2 T_s}{\partial y^2}\right) = 0. \tag{12}$$

The following variables are applied to render the above equations into the dimensionless

$$X = \frac{x}{H}, \quad U = \frac{uH}{\alpha_{bf}}, \quad Y = \frac{y}{H}, \quad V = \frac{vH}{\alpha_{bf}}, \quad \theta = \frac{T-T_c}{T_h-T_c}, \quad P = \frac{pL^2}{\rho_{bf}\alpha_{bf}^2},$$
$$Pr = \frac{\nu_{bf}}{\alpha_{bf}}, \quad Ra = \frac{g\beta_{bf}(T_h-T_c)L^3}{\alpha_{bf}\nu_{bf}}, \quad \theta_s = \frac{T_s-T_c}{T_h-T_c}, \quad Da = \frac{K}{H^2}.$$

The dimensionless reduced form of the governing equations are expressed as follows:
For the non-Newtonian nanofluid layer:

$$\frac{\partial U}{\partial X} + \frac{\partial V}{\partial Y} = 0, \tag{13}$$

$$\frac{\rho_{hnf}}{\rho_{bf}}\left(U\frac{\partial U}{\partial X} + V\frac{\partial U}{\partial Y}\right) = -\frac{\partial P}{\partial X} + \frac{\mu_{hnf}}{\mu_{bf}}Pr\left(2\frac{\partial}{\partial X}\left(\frac{\mu_a}{m}\frac{\partial U}{\partial X}\right) + \frac{\partial}{\partial Y}\left(\frac{\mu_a}{m}\left(\frac{\partial U}{\partial Y} + \frac{\partial V}{\partial X}\right)\right)\right), \tag{14}$$

$$\frac{\rho_{hnf}}{\rho_{bf}}\left(U\frac{\partial V}{\partial X} + V\frac{\partial V}{\partial Y}\right) = -\frac{\partial P}{\partial Y} + \frac{\mu_{hnf}}{\mu_{bf}}Pr\left(2\frac{\partial}{\partial Y}\left(\frac{\mu_a}{m}\frac{\partial V}{\partial Y}\right) + \frac{\partial}{\partial X}\left(\frac{\mu_a}{m}\left(\frac{\partial U}{\partial Y} + \frac{\partial V}{\partial X}\right)\right)\right) + \frac{(\rho\beta)_{hnf}}{(\rho\beta)_{bf}}PrRa\theta, \tag{15}$$

$$U\frac{\partial \theta}{\partial X} + V\frac{\partial \theta}{\partial Y} = \frac{\alpha_{hnf}}{\alpha_{bf}}\left(\frac{\partial^2 \theta}{\partial X^2} + \frac{\partial^2 \theta}{\partial Y^2}\right), \tag{16}$$

$$\mu_\alpha = m\left[2\left\{\left(\frac{\partial U}{\partial X}\right)^2 + \left(\frac{\partial V}{\partial Y}\right)^2\right\} + \left(\frac{\partial V}{\partial X} + \frac{\partial U}{\partial Y}\right)^2\right]^{\frac{n-1}{2}}. \tag{17}$$

For the Newtonian nanofluid porous layer:

$$\frac{\partial U}{\partial X} + \frac{\partial V}{\partial Y} = 0, \tag{18}$$

$$\frac{1}{\epsilon^2}\left(\frac{\rho_{hnf}}{\rho_{bf}}\right)\left(U\frac{\partial U}{\partial X} + V\frac{\partial U}{\partial Y}\right) = -\frac{\partial P}{\partial X} + \frac{1}{\epsilon}\frac{\mu_{hnf}}{\mu_{bf}}Pr\left(\frac{\partial^2 U}{\partial X^2} + \frac{\partial^2 U}{\partial Y^2}\right) + B_x, \tag{19}$$

$$\frac{1}{\epsilon^2}\left(\frac{\rho_{hnf}}{\rho_{bf}}\right)\left(U\frac{\partial V}{\partial X} + V\frac{\partial V}{\partial Y}\right) = -\frac{\partial P}{\partial Y} + \frac{1}{\epsilon}\frac{\mu_{hnf}}{\mu_{bf}}Pr\left(\frac{\partial^2 V}{\partial X^2} + \frac{\partial^2 V}{\partial Y^2}\right) + B_y + PrRa\theta\frac{(\rho\beta)_{hnf}}{(\rho\beta)_{bf}}, \tag{20}$$

$$U\frac{\partial \theta}{\partial X} + V\frac{\partial \theta}{\partial Y} = \frac{\alpha_{hnf}}{\alpha_{bf}}\left(\frac{\partial^2 \theta}{\partial X^2} + \frac{\partial^2 \theta}{\partial Y^2}\right). \tag{21}$$

where $B = (B_x, B_y)$ is known the force term caused by porosity. It is assumed through the following equation:

$$(B_x, B_y) = \frac{\mu_{hnf}}{\rho_{bf}\nu_{bf}} \frac{Pr}{Da}(U, V) - \frac{\rho_{hnf}}{\rho_{bf}} \frac{F_c}{\sqrt{Da}} \left(\sqrt{U^2 + V^2}\right)(U, V). \tag{22}$$

For the solid layer:

$$\frac{k_s}{k_{bf}} \left(\frac{\partial^2 \theta_s}{\partial X^2} + \frac{\partial^2 \theta_s}{\partial Y^2} \right) = 0. \tag{23}$$

The boundary conditions are as follows:

- Left wall: $U = 0, \quad V = 0, \quad \theta = 1;$
- right wall: $U = 0, \quad V = 0, \quad \theta = 0;$
- top/bottom wall: $U = 0, \quad V = 0, \quad \frac{\partial \theta}{\partial Y} = 0.$

2.3. Hybrid Thermophysical Properties

The effective physical properties of the hybrid nanofluid are evaluated using the flowing expressions [12,49,50]:

- Density: $\rho_{hnf} = (1 - \phi)\rho_f + \phi_{Ag}\rho_{Ag} + \phi_{MgO}\rho_{MgO};$
- Specific heat: $(\rho C_p)_{hnf} = (1 - \phi)(\rho C_p)_f + \phi_{Ag}(\rho C_p)_{Ag} + \phi_{MgO}(\rho C_p)_{MgO};$
- Coefficient of thermal expansion: $(\rho\beta)_{hnf} = (1 - \phi)(\rho\beta)_f + \phi_{Ag}(\rho\beta)_{Ag} + \phi_{MgO}(\rho\beta)_{MgO};$
- Thermal conductivity: $\frac{k_{hnf}}{k_f} = \frac{0.1745\times10^5 + \phi_{hnf}}{0.1747\times10^5 - 0.1498\times10^6\phi_{hnf} + 0.1117\times10^7\phi_{hnf}^2 + 0.1997\times10^8\phi_{hnf}^3};$
- Thermal diffusivity: $\alpha_{hnf} = \frac{k_{hnf}}{(\rho C_p)_{hnf}};$
- Effective dynamic viscosity: $\mu_{hnf} = (1 + 32.795\phi_{hnf} - 7214\phi_{hnf}^2 714600\phi_{hnf}^3$ $- 0.1941 \times 10^8\phi_{hnf}^4).$

Here, ϕ stands for the volume fraction of hybrid nanoparticles and is calculated by $\phi = \phi_{Ag} + \phi_{MgO}$.

2.4. The Nusselt Number

The Nu and Nu_{avg} for this study are derived as

$$Nu = -\frac{k_{hnf}}{k_f} \left(\frac{\partial \theta}{\partial Y} \right). \tag{24}$$

$$Nu_{\text{avg}} = \int_0^l Nu \, dX. \tag{25}$$

3. Numerical Plan

The model considered in (18)–(21) for a similar configuration was adopted here to numerically solve the governing equations based on the higher order GFEM. For the first step, a formulation called weak was established by taking an appropriate test space. After that, a hybrid mesh comprised of quadrilateral and triangular elements was generated to cover the whole domain of the considered configuration. The FEM based on the cubic polynomials (P3) was applied to compute for temperature and velocity fields, while the pressure was computed by the quadratic (P2) finite element space of functions. The robustness and stability of this higher order pair of FEM was confirmed in [51]. The discretized equations were simplified by employing the adaptive Newton's method. Some studies that have used the same solver can be found in the literature [52]. The solution is considered as satisfactory (convergence) when the following criterion is satisfied:

$$\frac{\sum_{i=1}^{m}\sum_{j=1}^{n}|\phi_{i,j}^{r+1}-\phi_{i,j}^{r}|}{\sum_{i=1}^{m}\sum_{j=1}^{n}|\phi_{i,j}^{r+1}|}\leq 10^{-6}, \tag{26}$$

where ϕ represents all the variables, i and j indicates the ith and jth grid and the superscript r is the rth iteration. m and n are the total number of nodes. The structure of the grid of the present computation can be seen in Figure 2.

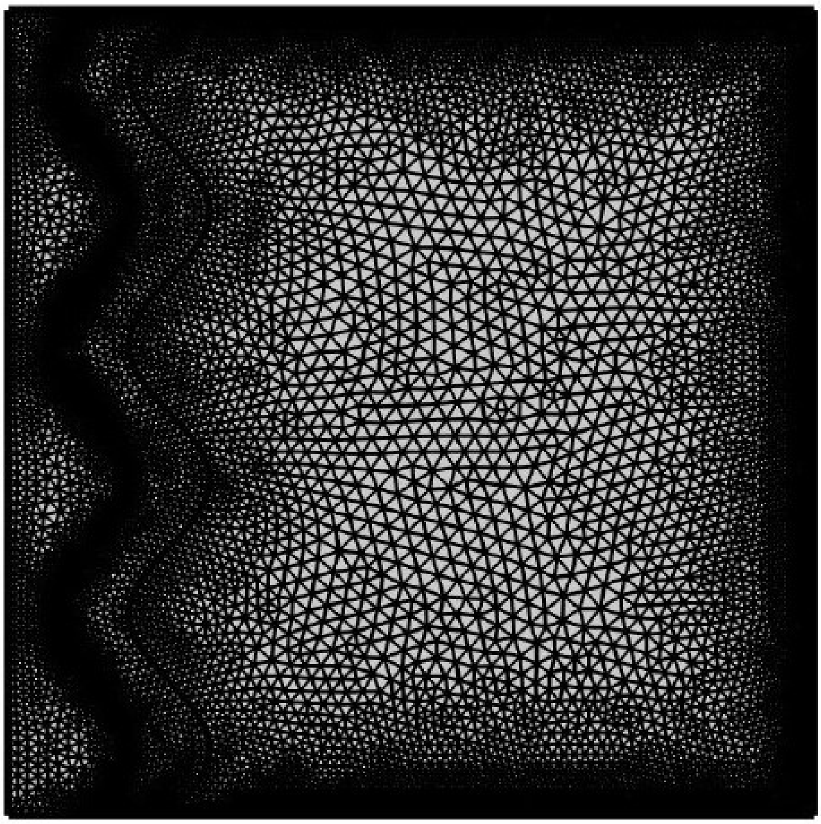

Figure 2. Coarsest mesh designed for the computational domain.

Code Authentication

To check the grid sensitivity, 9 different refined grids have been tested as shown in Table 2. The NEL and the DOFs were varied from 449–8535 to 19,383–328,959. As can be seen from the data in this table, a slight variation among the results of average Nu has been observed among 7 and 8 levels, respectively. Then, to avoid the long computational time, the retained mesh for this study was taken at level 8.

The present numerical model has been validated by comparing with [53,54] and also with the experimental data of the average Nu presented by [55] at the boundary conditions. As presented in Table 3, a good agreement is noted; in addition, the present results bear a close resemblance to those of [53–55].

Table 2. The test for grid convergence.

ℓ	NEL	DOFs	Nu_{avg}
1	449	8535	2.47491332
2	663	12,560	2.47642591
3	1110	19,844	2.47643410
4	1823	32,360	2.47665501
5	2364	41,987	2.47669507
6	3685	64,517	2.47675383
7	7378	129,730	2.47681493
8	19,383	328,959	2.47683835

Table 3. Code validation.

ϕ	Present	Shulepova et al. [53]	Saghir et al. [54]	Ho (Eeperimental) et al. [55]
1%	30.6594	31.6043	30.6570	32.2037
2%	30.5063	31.2538	30.5030	31.0905
3%	30.2179	30.8290	30.2050	29.0769

4. Results and Discussion

The results are presented for different numerical simulation cases, which are discussed below:

4.1. Streamlines and Isotherms for Different Parameters

Figures 3 and 4 are the representations of streamline and isotherm contours, respectively, for the fixed parameters $Pr = 6.2, \phi = 0.01, Da = 10^{-3}, \epsilon = 1, N = 3, A = 0.05$ and $Kr = 1$. The interpretations of both the figures are illustrated one by one as follows.

Figure 3 demonstrates the streamline contours for different values of the power law index and Rayleigh number. The plots show that streamlines are magnified by increasing the Rayleigh number. At $n = 0.6$, the trend of streamlines seems to exclusively switch towards expansion as $\mid \Psi \mid_{max} = 1.324244, 5.974056$ and 15.286430 for $Ra = 10^4$ to 10^6, respectively. This shows how much convection has been enhanced inside the cavity by increasing the Ra in the presence of the power law index. The maximum stream function is found at $Ra = 10^6$. Furthermore, the streamlines squeeze as the power law index intensifies. At $Ra = 10^6$ and $n = 1.8$, the flow pattern significantly approaches towards the porous layer. A remarkable penetration is found in the direction of the porous layer of the hybrid nanofluid.

Figure 4 demonstrates the temperature contours for different values of power law indexes and Rayleigh numbers. It is noticed that when $Ra = 10^3$, isotherms seem to be parallel to each other. Rapidly, the increase in the temperature gradient is encountered by increasing the Rayleigh number. When $Ra = 10^4$ to 10^6, the flow regime converts from conductive to convective. Moreover, a thin thermal boundary layer is observed at $Ra = 10^6$, which means that Ra is playing an important role in the solid-fluid layer, which is along the hot wall. When Ra increases, the temperature on the solid wall noticeably decreases, and a significance temperature distribution in the cavity is noticed, leading to the intensification of the buoyancy forces and thus the enhancement of the heat transfer. A reduction in the temperature gradients is observed as the power law index is increased, since the thermal boundary layer on the hot wall becomes thicker, reflecting the reduction of heat transfer. It is noticed from the figures that, when $Ra = 10^5$ and n = 0.6–1.8, the isotherms are weaker as the power law index is increased to $T = 0.3$. It can be concluded that the heat transfer is proportional to the Rayleigh number and inversely proportional to the power law index.

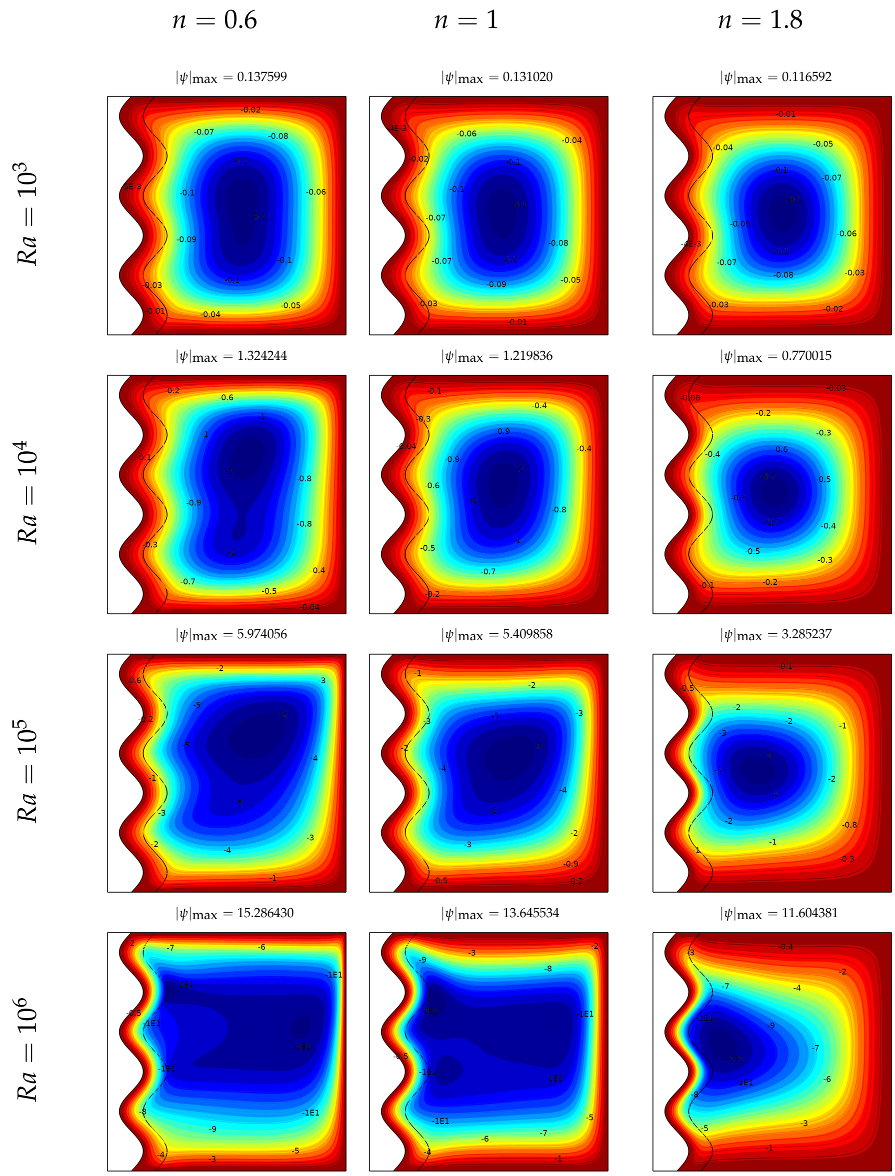

Figure 3. Streamlines for different values of power law indices n and Rayleigh numbers Ra.

Figures 5 and 6 are the demonstrations of the streamline and isotherms contours, respectively, for the fixed parameters $Pr = 6.2, \phi = 0.01, Ra = 10^5, \epsilon = 1, N = 3, A = 0.05$ and $Kr = 1$. The explanations of both the figures are illustrated one by one as follows.

Figure 5 represents the streamline contours for different values of the power law index and Darcy number. A marginal alteration is seen in the streamline pattern with increasing Da. At $Da = 10^{-2}$, a maximum value of the stream function is noted, which is $\mid \Psi \mid_{\max} = 6.339655$. This indicates that the fluid velocity is the highest at $n = 0.6$. The fluid circulation increases by enhancing Da. Moreover, a decreasing behaviour in the flow intensity is observed as the power law index rises. The flow pattern shrinks by varying n from $n = 0.6$ to $n = 1.8$. At $Da = 10^{-2}$, the flow pattern approaches the wavy walls significantly when $n = 1.8$, and the flow penetrates from the non-Newtonian hybrid layer to the porous hybrid nanofluid layer. This is a significant change that is noted at the specific parameters.

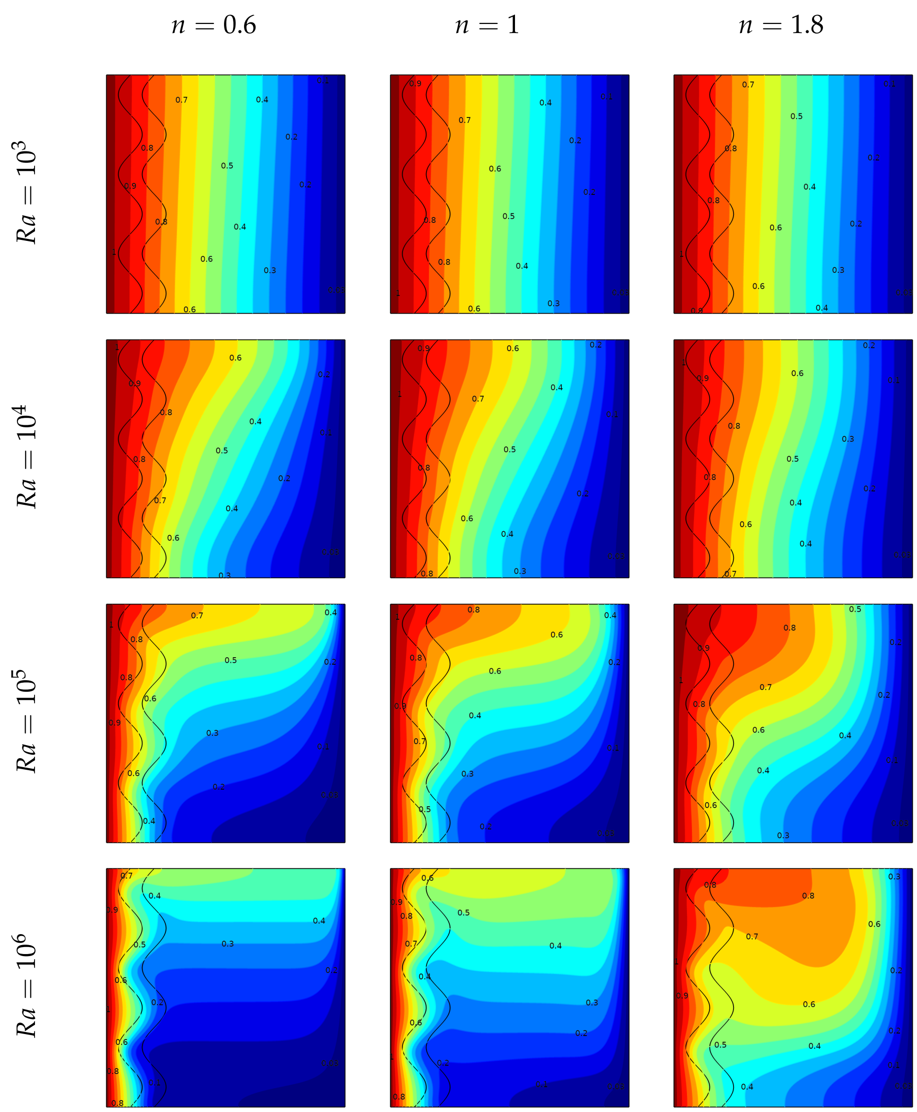

Figure 4. Isotherms for different values of power law indices n and Rayleigh numbers Ra.

Figure 6 demonstrates the temperature contours for different values of power law indexes and Darcy numbers. It is noticed that when $Da = 10^{-6}$ and $n = 0.6$, isotherms are quasi-parallel to the wavy interfaces. By increasing the Darcy number, a slow augmentation in heat transfer is observed, indicating that the heat transfer regime is shifting from conduction to convection mode. No considerable changes in the solid wall are observed due to the small fixed value of $Kr = 1$. It is to be noted that Kr is the ratio of the solid wall thermal conductivity to the hybrid nanofluid's thermal conductivity. A reduction in the temperature gradient is observed as the power law index increases, as seen in Figure 4, but tendency seems to be a little low here. The thermal layer alters from thinner to thicker, which reflects that the rate of heat transfer is low. At $Da = 10^{-4}$ and $Da = 10^{-2}$, the isotherm gradients are weaker with $T = 0.3$ and $T = 0.4$, respectively, as the power law index increases from 0.6 to 1.8.

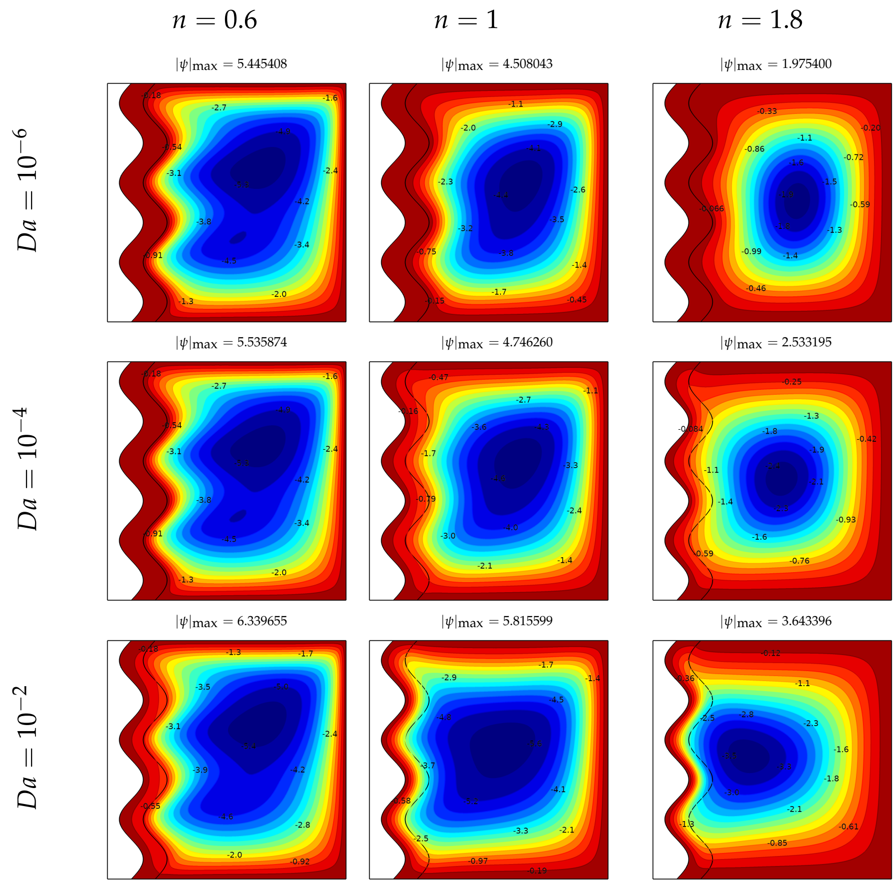

Figure 5. Streamlines for different values of power law indices n and Darcy numbers Da.

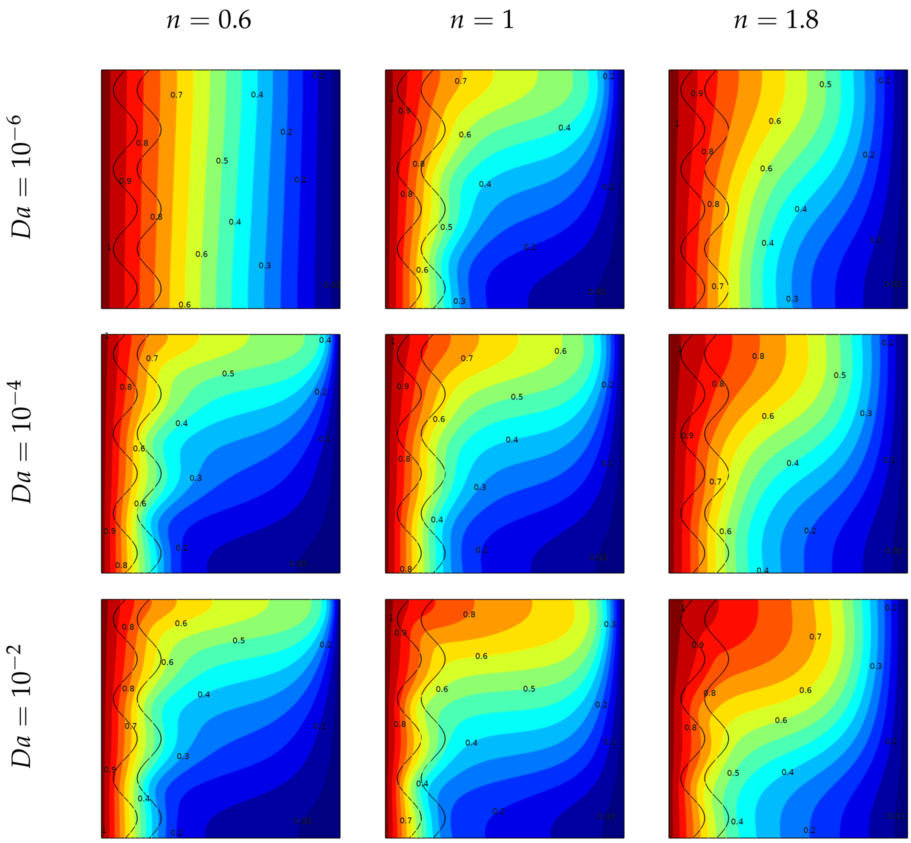

Figure 6. Isotherms for different values of power law indices n and Darcy numbers Da.

Figures 7 and 8 are the demonstrations of streamline and isotherm contours, respectively, for the fixed parameters $Pr = 6.2, \phi = 0.01, Ra = 10^5, Da = 10^{-3}, A = 0.05, \epsilon = 1$ and $Kr = 1$. The explanations of both the figures are illustrated one by one as follows.

Figure 7 represents the streamline contours for different values of the power law index and undulations. At $n = 0.6$, a little elongation is noticed in the streamline pattern by increasing the value of N. Gradually, the streamlines begin to occupy the whole area inside the cavity. It is confirmed from the $\mid \Psi \mid_{\max}$ values that fluid rotation changes into a slower mode inside the cavity by enhancing the undulations numbers from 1 to 3. Furthermore, the flow intensity is reduced when the power law index is augmented. The flow pattern shrinks, as seen in Figure 5, from $n = 0.8$ to 1.8. At $N = 1$, the flow pattern moves towards the porous layer from the non-Newtonian layer when $n = 1.8$.

Figure 8 demonstrates the temperature contours for different values of the power law index and undulations. By increasing the value of N, a slow augmentation in heat transfer is observed, indicating that the heat transfer mode gradually shifts from conduction to convection. The temperature profile in the solid fluid layer is not much effected by enhancing N due to the small value of the thermal conductivity ratio. Similarly to the previous cases, a reduction in the temperature gradients is observed as the power law index increases. The thermal layer is altered from thinner to thicker, which reflects that the rate of heat transfer is slow. At $N = 1$ and $N = 3$, the isotherms are weaker with $T = 0.2$ and $T = 0.3$, respectively, as the power law index increases from 0.6 to 1.8.

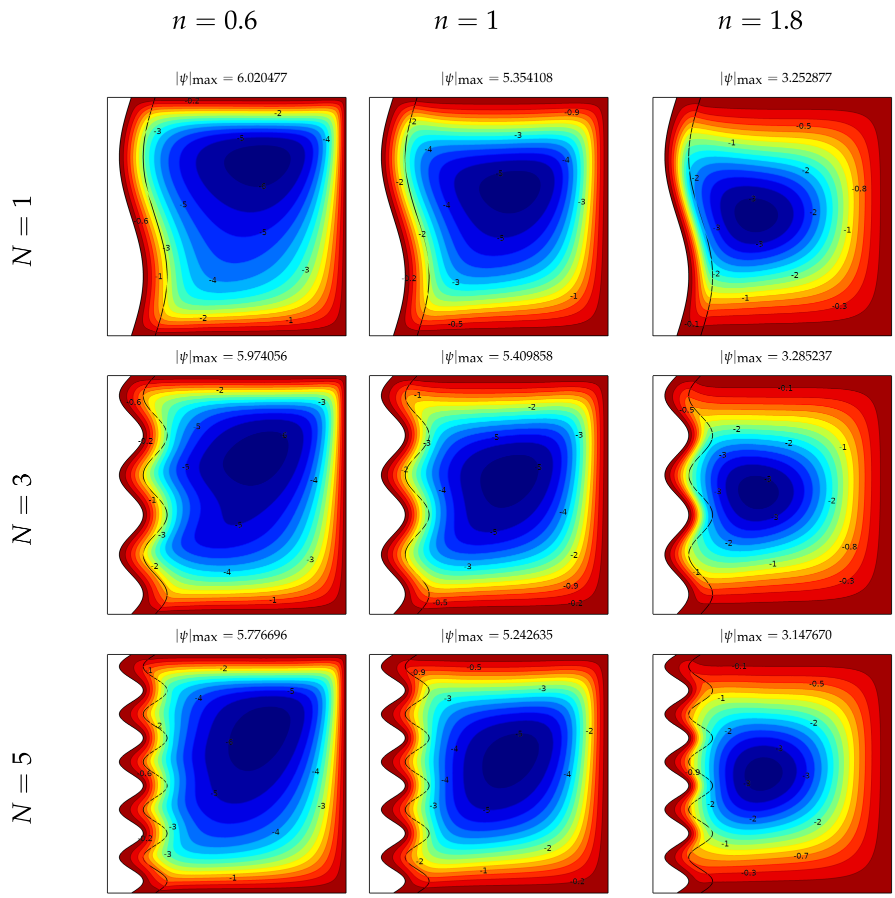

Figure 7. Streamlines for different values of power law indices n and undulations N.

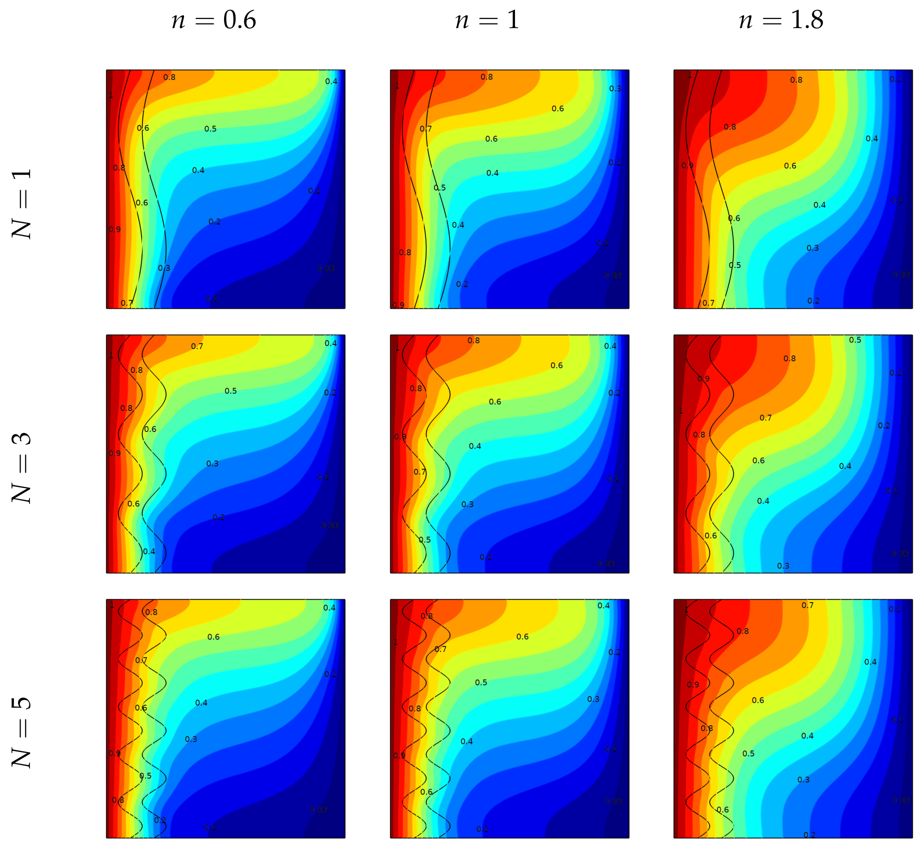

Figure 8. Isotherms for different values of power law indices n and undulations N.

4.2. Graphical Representations of Nusselt Number with Different Parameters

Figure 9a,b presents the variation for multifarious Ra numbers. It is noticeable that the local Nu intensifies significantly from $Ra = 10^5$ to 10^6.

Figure 9c,d presents the variation for multifarious Da numbers. It is noticed that the local Nu rises from $Da = 10^{-4}$ to 10^{-2}.

Figure 9e,f presents the variation for multifarious N numbers. It is observed that the local Nu increases for $N = 1$ and 2.

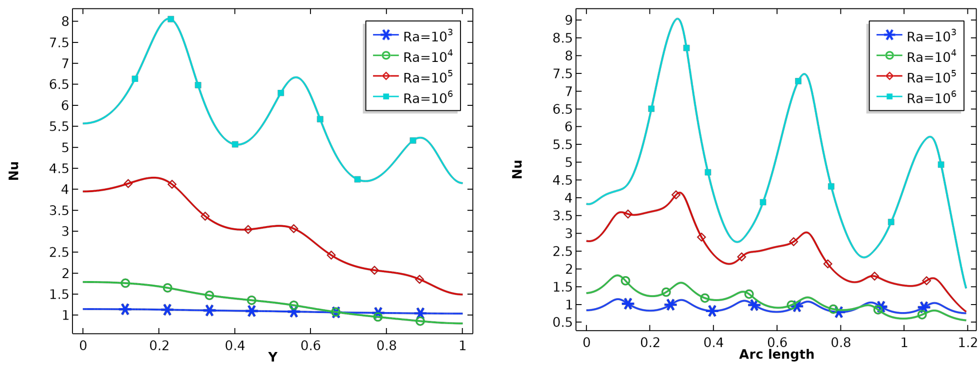

(**a**) (**b**)

Figure 9. *Cont.*

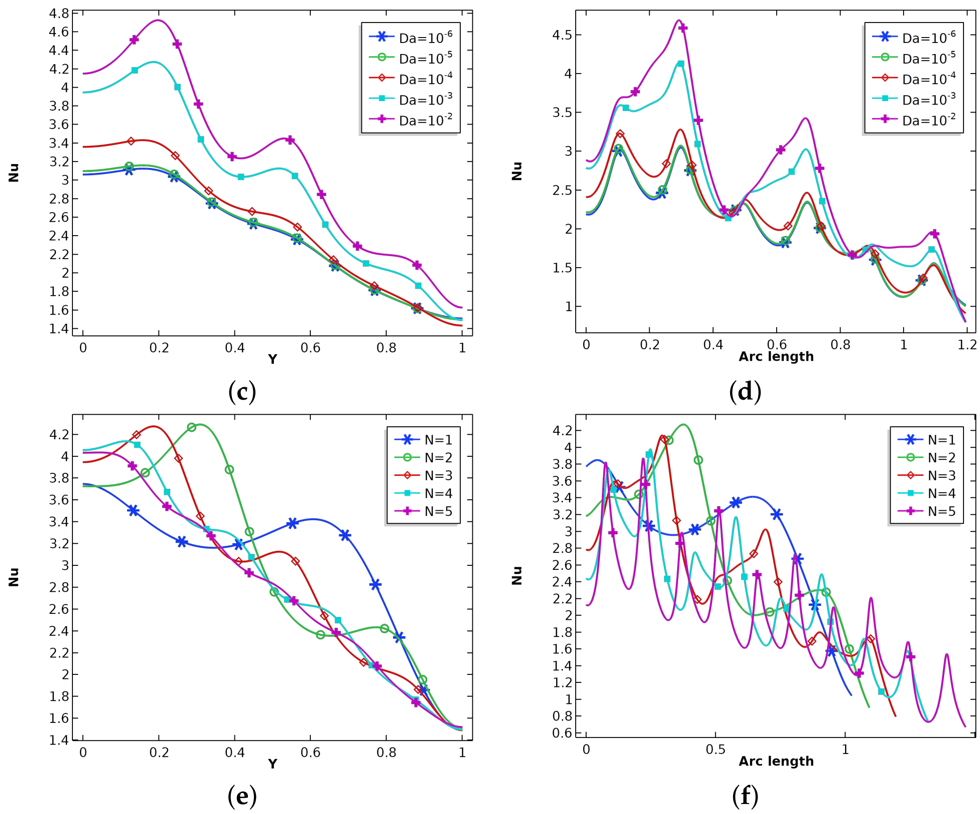

Figure 9. Local Nusselt number Nu for different values of Rayleigh, Darcy and Undulation numbers.

4.3. Tabular Representations of Average Nusselt Number with Different Parameters

Tables 4 and 5 depict Nu_{avg} values at the heated boundary and solid fluid interface, respectively, for different Ra values. From these tables, it can be observed that if Ra increases, the average Nu increases continuously, which reflect that convection heat transfer increases with Ra, as presented in the tables. On the other hand, a reverse behaviour of average Nu is observed by increasing the power law index.

Table 4. The values of the average Nusselt number (Nu_{avg}) at the heated boundary.

Ra	$n = 0.6$	$n = 1$	$n = 1.4$	$n = 1.8$
10^3	1.08714	1.08667	1.08633	1.08609
10^4	1.29168	1.23081	1.17212	1.13222
10^5	2.95847	2.61233	2.13034	1.70561
10^6	5.66139	5.04204	4.00963	3.07522

Table 5. The values of the average Nusselt number (Nu_{avg}) at the solid-fluid interface.

Ra	$n = 0.6$	$n = 1$	$n = 1.4$	$n = 1.8$
10^3	0.91016	0.90977	0.90948	0.90928
10^4	1.08140	1.03044	0.98130	0.94790
10^5	2.47684	2.18705	1.78353	1.42795
10^6	4.73973	4.22121	3.35687	2.57458

Tables 6 and 7 depict Nu_{avg} values at the heated boundary and solid fluid interface, respectively, for different Da values. It is noticeable from the tables that if Da increases slightly, the convective heat transfer rises proportionally.

Tables 8 and 9 depict Nu_{avg} values at the heated boundary and solid fluid interface, respectively, for different N values. It is noticeable from these tables that if N increases, the average Nu decreases slightly, which reflects that the heat transfer transfer is slow. Similar behaviour is observed versus the power law index. The results indicate that the heat transfer rate is reduced by increasing the undulation and power law index.

Table 6. The values of the average Nusselt number (Nu_{avg}) at the heated boundary.

Da	$n = 0.6$	$n = 1$	$n = 1.4$	$n = 1.8$
10^{-6}	2.40059	1.95070	1.54008	1.27267
10^{-5}	2.41455	1.97950	1.58761	1.31250
10^{-4}	2.52891	2.15096	1.77288	1.46036
10^{-3}	2.95847	2.61233	2.13034	1.70561
10^{-2}	3.21410	2.82162	2.26224	1.78898

Table 7. The values of the average Nusselt number (Nu_{avg}) at the solid-fluid interface.

Da	$n = 0.6$	$n = 1$	$n = 1.4$	$n = 1.8$
10^{-6}	2.00978	1.63313	1.28936	1.06548
10^{-5}	2.02147	1.65725	1.32916	1.09883
10^{-4}	2.11721	1.80079	1.48426	1.22262
10^{-3}	2.47684	2.18705	1.78353	1.42795
10^{-2}	2.69086	2.36227	1.89396	1.49774

Table 8. The values of the average Nusselt number (Nu_{avg}) at the heated boundary.

N	$n = 0.6$	$n = 1$	$n = 1.4$	$n = 1.8$
1	3.03071	2.68198	2.18358	1.73306
2	3.02175	2.67182	2.17879	1.74247
3	2.95847	2.61233	2.13034	1.70561
4	2.87997	2.54045	2.07793	1.67035
5	2.81333	2.48409	2.03873	1.64267

Table 9. The values of the average Nusselt number (Nu_{avg}) at the solid-fluid interface.

N	$n = 0.6$	$n = 1$	$n = 1.4$	$n = 1.8$
1	2.95900	2.61852	2.13192	1.69205
2	2.76620	2.44586	1.99453	1.59511
3	2.47684	2.18705	1.78353	1.42795
4	2.18071	1.92362	1.57341	1.26479
5	1.92207	1.69713	1.39286	1.12227

Tables 10 and 11 depict Nu_{avg} values at the heated boundary and solid fluid interface, respectively, for different A values. It is noticeable from these tables that if A increases, the average Nu decreases slightly. Similar behaviour is observed for the power law index. It can be mentioned that the rate of heat transfer is reduced by increasing the amplitude and power law index. It is to be noted that the rate of the reduction in the heat transfer is slow at the heated wall compared to the solid fluid interface. This is due to the existence of the porous layer.

Tables 12 and 13 depict Nu_{avg} values at the hot wall and solid fluid interface, respectively, for different $H2$ values. It can be seen that the thickness of the porous layer has a significant effect on the flow structure and heat transfer. As can be seen from these tables, if $H2$ increases, the average Nu decreases slightly. Similar behaviour is observed with an increase in the power law index. The tables indicates that the heat transfer is reduced by increasing the width of the porous layer and the power law index. It is noticed that the rate of reduction is lower at the heated wall compared to the solid fluid interface wall, as presented in Tables 10 and 11.

Table 10. The values of the average Nusselt number (Nu_{avg}) at the heated boundary.

A	$n = 0.6$	$n = 1$	$n = 1.4$	$n = 1.8$
0	3.00843	2.68445	2.20198	1.75516
0.01	3.00420	2.68110	2.20007	1.75379
0.02	2.99647	2.67194	2.19218	1.74860
0.03	2.98563	2.65717	2.17800	1.73916
0.04	2.97257	2.63714	2.15740	1.72498
0.05	2.95847	2.61233	2.13034	1.70561

Table 11. The values of the average Nusselt number (Nu_{avg}) at the solid-fluid interface.

A	$n = 0.6$	$n = 1$	$n = 1.4$	$n = 1.8$
0	3.00843	2.68445	2.20198	1.75516
0.01	2.97792	2.65765	2.18082	1.73845
0.02	2.89616	2.58250	2.11880	1.69006
0.03	2.77553	2.47019	2.02474	1.61678
0.04	2.63121	2.33430	1.90965	1.52689
0.05	2.47684	2.18705	1.78353	1.42795

Table 12. The values of the average Nusselt number (Nu_{avg}) at the heated boundary.

$H2$	$n = 0.6$	$n = 1$	$n = 1.4$	$n = 1.8$
0.15	3.02415	2.56662	1.99657	1.54771
0.2	2.95847	2.61233	2.13034	1.70561
0.25	2.91815	2.63164	2.20363	1.79797
0.3	2.89044	2.63491	2.23633	1.84533

Table 13. The values of the average Nusselt number (Nu_{avg}) at the solid-fluid interface.

$H2$	$n = 0.6$	$n = 1$	$n = 1.4$	$n = 1.8$
0.15	2.53183	2.14878	1.67153	1.29575
0.2	2.47684	2.18705	1.78353	1.42795
0.25	2.44309	2.20322	1.84489	1.50527
0.3	2.41989	2.20596	1.87226	1.54492

Tables 14 and 15 depict Nu_{avg} values at the heated boundary and solid fluid interface, respectively, for different thermal conductivity ratios Kr. The thermal conductivity ratio is defined as $Kr = \frac{Ks}{K_{hnf}}$. It is observed that a significant enhancement in heat transfer is gained by increasing Kr at the heated boundary. A slight reduction in the average Nu is observed by increasing the power law index. Similar behaviour regarding heat transfer is observed along the solid fluid interface, as shown in Table 15. The two tables reflect that convective heat transfer is more pronounced at the heated boundary compared to the solid fluid interface. This difference is due to the enhancement of the thermal conductivity by using the hybrid nanofluid. It can be concluded that at a high value of Kr, there is no tangible effect of the thermal resistance on both the heated boundary and the solid fluid interface. The heat transfer mode is changed from conductive to convective by increasing the conductivity ratio to $Kr = 10$.

Table 14. The values of the average Nusselt number (Nu_{avg}) at the heated boundary.

K_r	$n = 0.6$	$n = 1$	$n = 1.4$	$n = 1.8$
0.1	0.43974	0.36794	0.27694	0.20603
1	2.95846	2.61233	2.13034	1.70561
5	6.97416	6.54366	5.89804	5.24224
10	8.75246	8.39716	7.86149	7.29620

Table 15. The values of the average Nusselt number (Nu_{avg}) at the solid-fluid interface.

K_r	$n = 0.6$	$n = 1$	$n = 1.4$	$n = 1.8$
0.1	2.02479	1.69422	1.27521	0.94867
1	2.47683	2.18705	1.78353	1.42794
5	3.50113	3.28499	2.96084	2.63161
10	4.02660	3.86312	3.61665	3.35658

5. Conclusions

The impact of the power law index on natural convection has been investigated in the presence of three layers (solid, porous and non-Newtonian layers) in a 2D cavity using FEM. An Ag-MgO/water hybrid nanofluid was used for the porous and non-Newtonian layers. The effects of the governing parameters were studied, including the Rayleigh number, power law index, Darcy number, undulations, amplitude of the wavy interface, thickness of the layer and thermal conductivity ratio. Natural convection in porous media has a great interest in many technical and engineering applications. The main findings of the study can be summarised as follows:

- Streamlines are magnified by enhancing the Rayleigh number, and the maximum enlargement of the streamlines is found at $Ra = 10^6$;
- A remarkable penetration of streamlines is identified towards the porous hybrid layer by increasing the power law index;
- The temperature along the solid wall decreases and a significant distribution of temperature is noted in the remaining parts of the cavity by increasing Ra;
- The average Nusselt number increases by increasing Ra, and its maximum occurs at $Ra = 10^6$;
- No considerable alteration is observed for isotherms at the solid layer by increasing Da;
- The average Nusselt number decreases by increasing the undulation number;
- The average Nusselt number declines by increasing the thickness ($H2$) and the power law index n;
- The rate of heat transfer increases at the heated boundary and solid fluid interface by increasing the ratio of thermal conductivity;
- The temperature field at the solid wall is not considerably affected by increasing Da and N.

Author Contributions: M.O.: Formal analysis, Investigation, Writing original draft, Writing review and editing, Visualization. M.J.: Methodology, Software, Validation, Formal analysis, Investigation, Writing—review and editing. S.H.: Methodology, Software, Validation, Formal analysis, Investigation. L.K.: Formal analysis, Investigation, Writing review and editing, Supervision. C.M.: Investigation, Writing review and editing. All authors have read and agreed to the published version of the manuscript.

Funding: This project was funded by the Deanship of Scientific Research (DSR), King Abdulaziz University, Jeddah, Saudi Arabia, under grant No. (D-667-305-1441).

Institutional Review Board Statement: Not applicable.

Informed Consent Statement: Not applicable.

Data Availability Statement: Not applicable.

Acknowledgments: The authors are gratefully acknowledge DSR's technical and financial support.

Conflicts of Interest: The authors declare no conflict of interest.

Nomenclature

X, Y	Horizontal and vertical coordinates (dimensionless)
U, V	Velocity components (dimensionless)
g	Gravitational acceleration (m s^{-2})
K	Permeability of porous media (m^2)
C_p	Specific heat (J kg^{-1}K^{-1})
Da	Darcy number, K/L^2
Ra	Rayleigh number
x, y	Dimensional space coordinates (m)
u, v	Dimensional velocity components (m s^{-1})
Pr	Prandtl number, ν_f/α_f
T	temperature (K)
Greek symbols	
α	thermal diffusivity (m^2 s^{-1})
β	thermal expansion coefficient (K^{-1})
μ	dynamic viscosity (kg m^{-1}s^{-1})
ρ	density (kg m^{-3})

References

1. Khanafer, K.; Vafai, K. A critical synthesis of thermophysical characteristics of nanofluids. *Int. J. Heat Mass Transf.* **2011**, *54*, 4410–4428. [CrossRef]
2. Khodabandeh, E.; Safaei, M.R.; Akbari, S.; Akbari, O.A.; Alrashed, A.A. Application of nanofluid to improve the thermal performance of horizontal spiral coil utilized in solar ponds: Geometric study. *Renew. Energy* **2018**, *122*, 1–16. [CrossRef]
3. Koca, H.D.; Doganay, S.; Turgut, A.; Tavman, I.H.; Saidur, R.; Mahbubul, I.M. Effect of particle size on the viscosity of nanofluids: A review. *Renew. Sustain. Energy Rev.* **2018**, *82*, 1664–1674. [CrossRef]
4. Wang, X.Q.; Mujumdar, A.S. Heat transfer characteristics of nanofluids: A review. *Int. J. Therm. Sci.* **2007**, *46*, 1–19. [CrossRef]
5. Punith Gowda, R.J.; Jyothi, A.M.; Naveen Kumar, R.; Prasannakumara, B.C.; Sarris, I.E. Convective Flow of Second Grade Fluid Over a Curved Stretching Sheet with Dufour and Soret Effects. *Int. J. Appl. Comput. Math.* **2021**, *7*, 226. [CrossRef]
6. Sarada, K.; Gowda, R.J.P.; Sarris, I.E.; Kumar, R.N.; Prasannakumara, B.C. Effect of Magnetohydrodynamics on Heat Transfer Behaviour of a Non-Newtonian Fluid Flow over a Stretching Sheet under Local Thermal Non-Equilibrium Condition. *Fluids* **2021**, *6*, 264. [CrossRef]
7. Punith Gowda, R.J.; Naveen Kumar, R.; Jyothi, A.M.; Prasannakumara, B.C.; Sarris, I.E. Impact of Binary Chemical Reaction and Activation Energy on Heat and Mass Transfer of Marangoni Driven Boundary Layer Flow of a Non-Newtonian Nanofluid. *Processes* **2021**, *9*, 702. [CrossRef]
8. Shankaralingappa, B.M.; Madhukesh, J.K.; Sarris, I.E.; Gireesha, B.J.; Prasannakumara, B.C. Influence of Thermophoretic Particle Deposition on the 3D Flow of Sodium Alginate-Based Casson Nanofluid over a Stretching Sheet. *Micromachines* **2021**, *12*, 1474. [CrossRef]
9. Gkountas, A.A.; Benos, L.T.; Sofiadis, G.N.; Sarris, I.E. A printed-circuit heat exchanger consideration by exploiting an Al_2O_3-water nanofluid: Effect of the nanoparticles interfacial layer on heat transfer. *Therm. Sci. Eng. Prog.* **2021**, *22*, 100818. [CrossRef]
10. Nield, D.A.; Bejan, A. *Convection in Porous Media*; Springer: New York, NY, USA, 2013; Volume 4.
11. Vafai, K. *Porous Media: Applications in Biological Systems and Biotechnology*; CRC Press: Amsterdam, The Netherlands, 2010.
12. Hemmat Esfe, M.; Abbasian Arani, A.A.; Rezaie, M.; Yan, W.M.; Karimipour, A. Experimental determination of thermal conductivity and dynamic viscosity of Ag-MgO/water hybrid nanofluid. *Int. Commun. Heat Mass Transf.* **2015**, *66*, 189–195. [CrossRef]
13. Hemmat Esfe, M.; Saedodin, S.; Biglari, M.; Rostamian, H. Experimental investigation of thermal conductivity of CNTs-Al_2O_3/water: A statistical approach. *Int. Commun. Heat Mass Transf.* **2015**, *69*, 29–33. [CrossRef]
14. Hemmat Esfe, M.; Yan, W.M.; Akbari, M.; Karimipour, A.; Hassani, M. Experimental study on thermal conductivity of DWCNT-ZnO/water-EG nanofluids. *Int. Commun. Heat Mass Transf.* **2015**, *68*, 248–251. [CrossRef]
15. Sheremet, M.; Pop, I.; Shenoy, A. Unsteady free convection in a porous open wavy cavity filled with a nanofluid using Buongiorno's mathematical model. *Int. Commun. Heat Mass Transf.* **2015**, *67*, 66–72. [CrossRef]
16. Sheremet, M.; Pop, I. Conjugate natural convection in a square porous cavity filled by a nanofluid using Buongiorno's mathematical model. *Int. J. Heat Mass Transf.* **2014**, *79*, 137–145. [CrossRef]
17. Sheremet, M.; Pop, I.; Bachok, N. Effect of thermal dispersion on transient natural convection in a wavy-walled porous cavity filled with a nanofluid: Tiwari and Das' nanofluid model. *Int. J. Heat Mass Transf.* **2016**, *92*, 1053–1060. [CrossRef]
18. Shenoy, A.; Sheremet, M.; Pop, I. *Convective Flow and Heat Transfer From Wavy Surfaces: Viscous Fluids, Porous Media, and Nanofluids*; CRC Press: Amsterdam, The Netherlands, 2016; pp. 1–306. [CrossRef]
19. Hoghoughi, G.; Izadi, M.; Oztop, H.F.; Abu-Hamdeh, N. Effect of geometrical parameters on natural convection in a porous undulant-wall enclosure saturated by a nanofluid using Buongiorno's model. *J. Mol. Liq.* **2018**, *255*, 148–159. [CrossRef]

20. Miroshnichenko, I.; Sheremet, M. Numerical study of turbulent natural convection in a cube having finite thickness heat-conducting walls. *Heat Transf. Res.* **2015**, *51*, 1559–1569. [CrossRef]
21. Chamkha, A.J.; Ismael, M.A. Conjugate heat transfer in a porous cavity filled with nanofluids and heated by a triangular thick wall. *Int. J. Therm. Sci.* **2013**, *67*, 135–151. [CrossRef]
22. Kuznetsov, G.; Sheremet, M. Unsteady natural convection of nanofluids in an enclosure having finite thickness walls. *Comput. Therm. Sci.* **2011**, *3*, 427–443. [CrossRef]
23. Xiong, P.Y.; Khan, M.; Punith Gowda, R.; Kumar, R.; Prasannakumara, B.C.; Chu, Y.M. Comparative analysis of (Zinc ferrite, Nickel Zinc ferrite) hybrid nanofluids slip flow with entropy generation. *Mod. Phys. Lett. B* **2021**, *35*, 2150342. [CrossRef]
24. Alsabery, A.; Chamkha, A.; Hussain, S.; Saleh, H.; Hashim, I. Heatline visualization of natural convection in a trapezoidal cavity partly filled with nanofluid porous layer and partly with non-Newtonian fluid layer. *Adv. Powder Technol.* **2015**, *26*, 1230–1244. [CrossRef]
25. Rashid, Q.; Ali, F. Effects of Prandtl Number on Natural Convection in a Cavity Filled with Silver/Water Nanofluid-Saturated Porous Medium and Non-Newtonian Fluid Layers Separated by Sinusoidal Vertical Interface. *Arab. J. Sci. Eng.* **2019**, *44*, 10339–10354.
26. Khezzar, L.; Siginer, D.; Vinogradov, I. Natural convection of power law fluids in inclined cavities. *Int. J. Therm. Sci.* **2012**, *53*, 8–17. [CrossRef]
27. Kefayati, G. Simulation of non-Newtonian molten polymer on natural convection in a sinusoidal heated cavity using FDLBM. *J. Mol. Liq.* **2014**, *195*, 165–174. [CrossRef]
28. Wu, W.T.; Massoudi, M. Recent Advances in Mechanics of Non-Newtonian Fluids. *Fluids* **2020**, *5*, 10. [CrossRef]
29. Mamou, M.; Lamsaadi, M.; Naimi, M.; Hasnaoui, M. Natural Convection in a Vertical Rectangular Cavity Filled with a Non-Newtonian Power Law Fluid and Subjected to Horizontal Temperature Gradient. *Numer. Heat Transf. Part A Appl.* **2006**, *49*, 969–990. [CrossRef]
30. Lamsaadi, M.; Naïmi, M.; Hasnaoui, M. Natural convection of non-Newtonian power law fluids in a shallow horizontal rectangular cavity uniformly heated from below. *Heat Mass Transf.-Stoffuebertragung* **2005**, *41*, 239–249. [CrossRef]
31. Alsabery, A.; Chamkha, A.; Saleh, H.; Hashim, I. Natural Convection Flow of a Nanofluid in an Inclined Square Enclosure Partially Filled with a Porous Medium. *Sci. Rep.* **2017**, *7*, 2357. [CrossRef]
32. Chamkha, A.; Ismael, M. Natural Convection in Differentially Heated Partially Porous Layered Cavities Filled with a Nanofluid. *Numer. Heat Transf. Part A Appl.* **2014**, *65*, 1089–1113. [CrossRef]
33. Li, Y.M.; Al-Khaled, K.; Gouadria, S.; El-Zahar, E.R.; Usman; Khan, S.U.; Khan, M.I.; Malik, M.Y. Numerical simulations for three-dimensional rotating porous disk flow of viscoelastic nanomaterial with activation energy, heat generation and Nield boundary conditions. *Waves Random Complex Media* **2022**, 1–20. [CrossRef]
34. Lin, P.; Ghaffari, A. Steady flow and heat transfer of the power-law fluid between two stretchable rotating disks with non-uniform heat source/sink. *J. Therm. Anal. Calorim.* **2020**, *146*, 1735–1749. [CrossRef]
35. Song, Y.Q.; Khan, M.I.; Qayyum, S.; Gowda, R.J.P.; Kumar, R.N.; Prasannakumara, B.C.; Elmasry, Y.; Chu, Y.M. Physical impact of thermo-diffusion and diffusion-thermo on Marangoni convective flow of hybrid nanofluid ($MnZiFe_2O_4$–$NiZnFe_2O_4$–H_2O) with nonlinear heat source/sink and radiative heat flux. *Mod. Phys. Lett. B* **2021**, *35*, 2141006. [CrossRef]
36. Alsabery, A. Inclination Angle Effect on Natural Convection in a Square Cavity Partially Filled with Non-Newtonian Fluids Layer. In Proceedings of the 2015 UKM FST Postgraduate Colloquium, Bangi, Malaysia, 15–16 April 2015; Volume 1678. [CrossRef]
37. Tuan, N.; Mahmoud Aly, A.; Lee, S.W. Effect of a wavy interface on the natural convection of a nanofluid in a cavity with a partially layered porous medium using the ISPH method. *Numer. Heat Transf. Part A Appl.* **2017**, *72*, 68–88. [CrossRef]
38. Al-Srayyih, B.M.; Gao, S.; Hussain, S.H. Effects of linearly heated left wall on natural convection within a superposed cavity filled with composite nanofluid-porous layers. *Adv. Powder Technol.* **2019**, *30*, 55–72. [CrossRef]
39. Khafaji, S. Effect of Layer Thickness on Natural Convection in a Square Enclosure Superposed by Nano-Porous and Non-Newtonian Fluid Layers Divided by a Wavy Permeable Wall. *Int. J. Mech. Mechatron. Eng.* **2019**, *19*, 26–49.
40. Cho, C.C.; Chen, C.L.; Hwang, J.; Chen, C.K. Natural Convection Heat Transfer Performance of Non-Newtonian Power-Law Fluids Enclosed in Cavity With Complex-Wavy Surfaces. *J. Heat Transf.* **2013**, *136*, 014502. [CrossRef]
41. Kefayati, G.; Tang, H. MHD thermosolutal natural convection and entropy generation of Carreau fluid in a heated enclosure with two inner circular cold cylinders, using LBM. *Int. J. Heat Mass Transf.* **2018**, *126*, 508–530. [CrossRef]
42. Saleh, H.; Alsabery, A.I.; Hashim, I. Natural convection in polygonal enclosures with inner circular cylinder. *Adv. Mech. Eng.* **2015**, *7*, 1687814015622899. [CrossRef]
43. Turan, O.; Sachdeva, A.; Chakraborty, N.; Poole, R.J. Laminar natural convection of power-law fluids in a square enclosure with differentially heated side walls subjected to constant temperatures. *J. Non-Newton. Fluid Mech.* **2011**, *166*, 1049–1063. [CrossRef]
44. Barnoon, P.; Toghraie, D.; Dehkordi, R.B.; Afrand, M. Two phase natural convection and thermal radiation of Non-Newtonian nanofluid in a porous cavity considering inclined cavity and size of inside cylinders. *Int. Commun. Heat Mass Transf.* **2019**, *108*, 104285. [CrossRef]
45. Soltani, O.; Akbari, M. Effects of temperature and particles concentration on the dynamic viscosity of MgO-MWCNT/ethylene glycol hybrid nanofluid: Experimental study. *Phys. E Low-Dimens. Syst. Nanostruct.* **2016**, *84*, 564–570. [CrossRef]
46. Ghalambaz, M.; Doostani, A.; Izadpanahi, E.; Chamkha, A.J. Conjugate natural convection flow of Ag–MgO/water hybrid nanofluid in a square cavity. *J. Therm. Anal. Calorim.* **2020**, *139*, 2321–2336. [CrossRef]

47. Kefayati, G. Simulation of magnetic field effect on natural convection of non-Newtonian power-law fluids in a sinusoidal heated cavity using FDLBM. *Int. Commun. Heat Mass Transf.* **2014**, *53*, 139–153. [CrossRef]
48. Kefayati, G. Lattice Boltzmann simulation of double-diffusive natural convection of viscoplastic fluids in a porous cavity. *Phys. Fluids* **2019**, *31*, 013105. [CrossRef]
49. Nasrin, R.; Alim, M. Free convective flow of nanofluid having two nanoparticles inside a complicated cavity. *Int. J. Heat Mass Transf.* **2013**, *63*, 191–198. [CrossRef]
50. Hussain, S.; Tayebi, T.; Armaghani, T.; Rashad, A.M.; Nabwey, H.A. Conjugate natural convection of non-Newtonian hybrid nanofluid in wavy-shaped enclosure. *Appl. Math. Mech.* **2022**, *43*, 447–466. [CrossRef]
51. Hussain, S.; Schieweck, F.; Turek, S. Efficient Newton-multigrid solution techniques for higher order space–time Galerkin discretizations of incompressible flow. *Appl. Numer. Math.* **2014**, *83*, 51–71. [CrossRef]
52. Hussain, S.; Mehmood, K.; Sagheer, M.; Farooq, A. Entropy generation analysis of mixed convective flow in an inclined channel with cavity with Al_2O_3-water nanofluid in porous medium. *Int. Commun. Heat Mass Transf.* **2017**, *89*, 198–210. [CrossRef]
53. Shulepova, E.V.; Sheremet, M.A.; Oztop, H.F.; Abu-Hamdeh, N. Mixed convection of Al_2O_3-H_2O nanoliquid in a square chamber with complicated fin. *Int. J. Mech. Sci.* **2020**, *165*, 105192. [CrossRef]
54. Saghir, M.Z.; Ahadi, A.; Mohamad, A.; Srinivasan, S. Water aluminum oxide nanofluid benchmark model. *Int. J. Therm. Sci.* **2016**, *109*, 148–158. [CrossRef]
55. Ho, C.; Liu, W.; Chang, Y.; Lin, C. Natural convection heat transfer of alumina-water nanofluid in vertical square enclosures: An experimental study. *Int. J. Therm. Sci.* **2010**, *49*, 1345–1353. [CrossRef]